日本磁気学会
ISSN 2432-0250
Journal of the Magnetics Society of Japan
Electronic Journal URL: https://www.jstage.jst.go.jp/browse/msjmag

Vol.42 No.1　2018

Journal

JOURNAL OF THE MAGNETICS SOCIETY OF JAPAN

Vol.42 No.1 2018

日本磁気学会

ISSN 2432-0250

HP: http://www.magnetics.jp/ e-mail: msj@bj.wakwak.com
Electronic Journal: http://www.jstage.jst.go.jp/browse/msjmag

有限要素法解析ソフトウェア COMSOL Multiphysics®

COMSOL MULTIPHYSICS®

マルチフィジックスの進化論

無制限・強連成で実現象に即したシミュレーション事例のご紹介

永久磁石を利用した磁気軸受の解析例

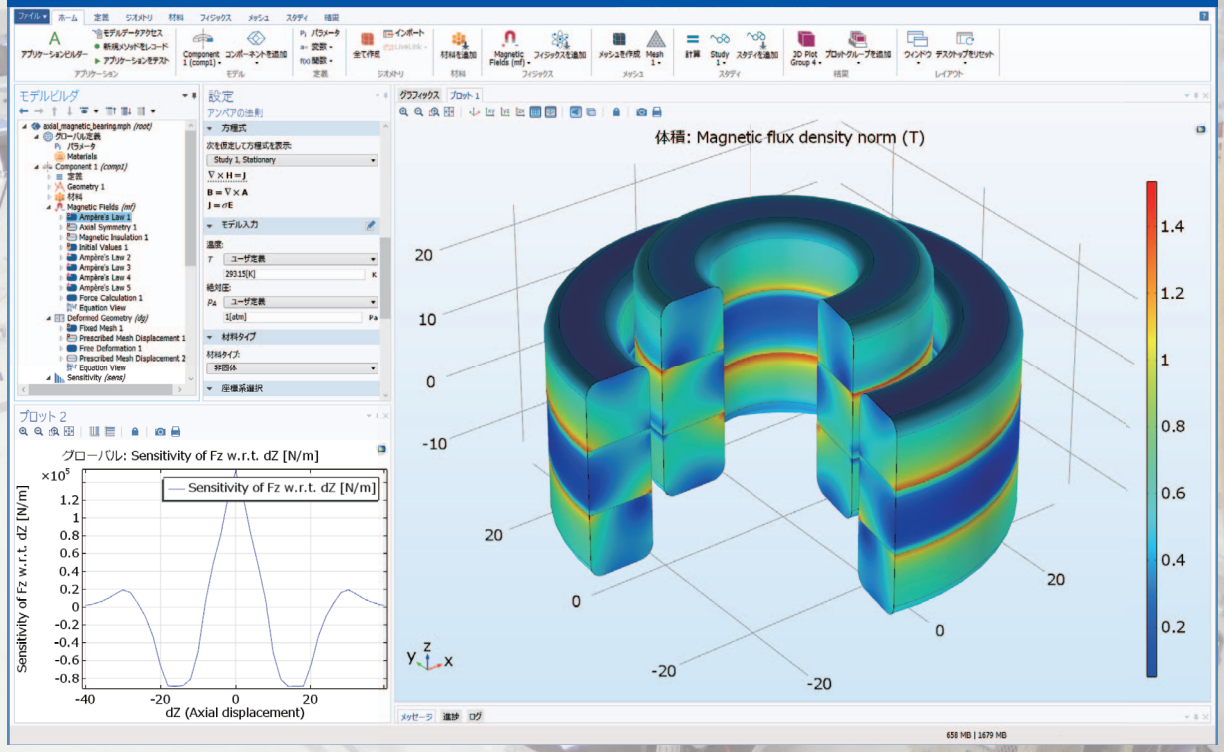

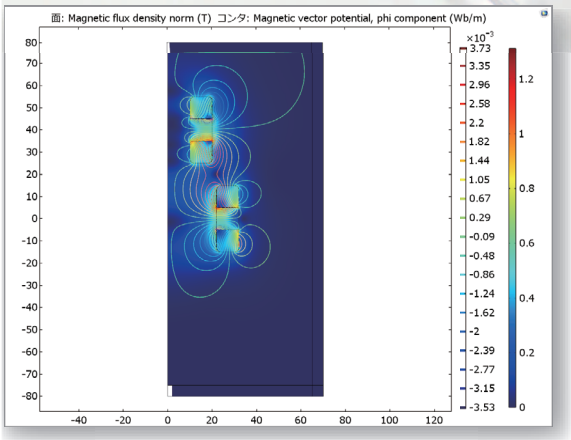

永久磁石を使用した磁気軸受

永久磁石を使用した軸受はターボ機械、ポンプ、モータ、発電機やフライホイール式エネルギー貯蔵システムなど、様々な分野で使用されています。非接触かつ潤滑不要で保守整備を大幅に省略できる点は、従来の機械式ベアリングと比べて重要なメリットです。
この例では、軸方向の永久磁石軸受の磁気力と剛性などの設計パラメータを計算する方法を示しています。

※AC/DCモジュールはCOMSOL Multiphysicsと併用するアドオン製品です。

AC/DC モジュールの適用例

- AC/DC 電流分布、電場分布
- バイオヒーティング
- コイルとソレノイド
- SPICE 回路とフィールドシミュレーション
- 接触抵抗
- 電磁両立性 (EMC) および電磁妨害 (EMI)
- 電磁力およびトルク
- 電磁力シールド
- 電気機械の変形
- ホール効果を利用したセンサ
- インシュレータ、コンデンサ、誘電体
- モータ、ジェネレータ、および他の電気機械
- 非線形材料
- 寄生容量とインダクタンス
- 永久磁石と電磁石
- 多孔質材料
- 抵抗および誘導加熱
- センサ
- 超伝導体
- 変圧器とインダクタ

COMSOL Multiphysics® なら、今まで不可能だった 3 種以上のマルチフィジックス解析を強連成で実現できます。30 日間全機能無料トライアル、無料の導入セミナー、1000種を超える世界の様々な事例をご提供いたします。詳しくは、下記の弊社営業部までお問い合せください。

COMSOL

http://www.comsol.jp

KESCO KEISOKU ENGINEERING SYSTEM
計測エンジニアリングシステム株式会社
http://www.kesco.co.jp/comsol/
Tel : 03-5282-7040 • Fax : 03-5282-0808

新型 磁区観察顕微鏡 シリーズ

小型磁区観察顕微鏡

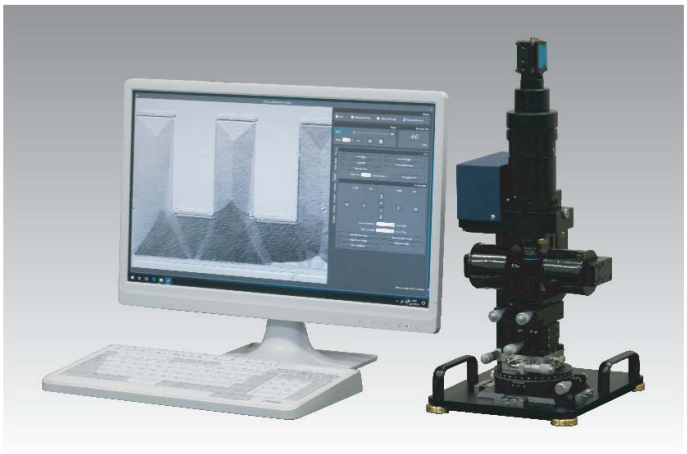

Neomagnesia Lite

※概要・特長

- 磁区観察ユニットに電磁石、 ステージ、 励磁電源、ソフトウェアを組み合わせたトータルシステム
- 従来の弊社の磁区観察顕微鏡から大幅なプライスダウンを実現
- 磁区の動的な観察を可能とする高機能な専用ソフトウェアが付属
- 最大で 1kOe（面内方向）の磁場を印加可能
- 本体の大きさは 210×260×475mm^3、 質量も 8kg と軽量・コンパクト
- 白色 LED 光源の採用により高安定・長寿命

磁区観察ユニット

※概要・特長

- プローバ装置などに取り付けることが可能な小型・低価格の磁区観察ユニット
- 面内 / 垂直どちらの磁化方向にも対応
- 社内設計光学系による面内磁区の高コントラスト観察（空間分解能 3μm 以下 ）
- 光学系ヘッドの大きさは 150×150×300mm^3、質量も 2kg と軽量・コンパクト
- 白色 LED 光源の採用により高安定・長寿命
- オプションとして顕微鏡スタンド・ステージ・高機能観察 / 解析ソフトウェアなどを用意

この製品以外に、 30 年の研究現場への対応経験に基づいた高精度・高性能の磁気 Kerr 効果装置、Faraday 装置、 磁区観察顕微鏡など、 各種磁気光学製品の取り揃えがございます。
お気軽にお問合せください。

レーザとレーザ応用システム製品の総合メーカー
NEOARK ネオアーク株式会社
営 業 部 / 〒156-0041 東京都世田谷区大原2-17-6-108 TEL(03)6379-5539 FAX(03)6379-5688
大阪支店 / 〒541-0056 大阪市中央区久太郎町2-3-8-201 TEL(06)6271-5123 FAX(06)6271-5110
本社 第1工場・第2工場 / 八王子市
URL http://www.neoark.co.jp E-mail:info@neoark.co.jp

INDEX

世界初！
高温超電導型VSM

新製品

世界初*、高温超電導マグネットをVSMに採用することで
測定速度 当社従来機1/20を実現。
0.5mm cube磁石のBr, HcJ高精度測定が可能と
なりました。
*2014年7月 東英工業調べ

測定結果例

高温超電導VSMによるNdFeB(sint.) 0.5mm cube BHカーブ

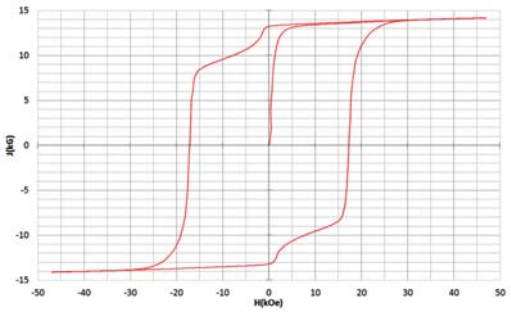

磁化測定レンジ：0.2emu
Br = 13.2kG　　HcJ = 17.2kOe

高温超電導VSMによるNdFeB(sint.) 1mm cube BHカーブ

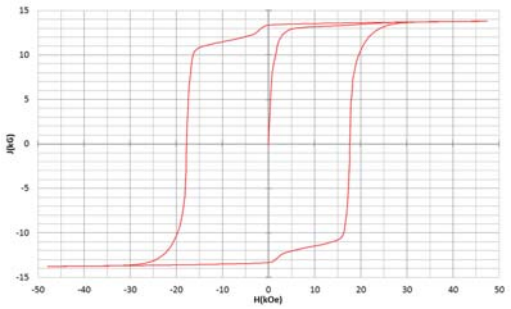

磁化測定レンジ：2emu
Br = 13.3kG　　HcJ = 17.7kOe

高温超電導VSMによるNdFeB(sint.) 4mm cube BHカーブ

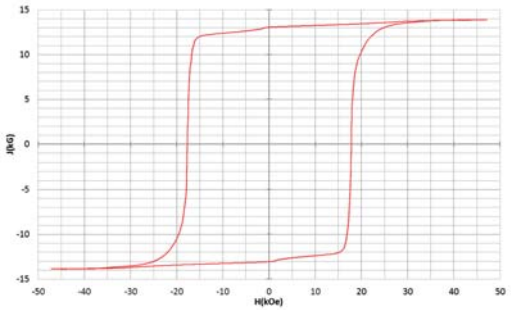

磁化測定レンジ：100emu
Br = 13.1kG　　HcJ = 17.8kOe

高速測定を実現

高温超電導マグネット採用により、高速測定を実現しました。Hmax= 5Tesla, Full Loop 測定が2分で可能です。
（当社従来機：Full Loop測定　40分）

小試料のBr,HcJ高精度測定

0.5mm cube 磁石のBr,HcJ高精度測定ができ、表面改質領域を切り出しBr,HcJの強度分布等、微小変化量の比較測定が可能です。
また、試料の加工劣化の比較測定が可能です。

試料温度可変測定

−50℃～+200℃温度可変UNIT（オプション）

磁界発生部の小型化

マグネットシステム部寸法：0.8m×0.3m×0.3m

TOEI 東英工業株式会社
http://www.toeikogyo.co.jp
〒194-0035 東京都町田市忠生1-8-13
TEL：042-791-1211 FAX：042-792-0490
E-mail : sales@toeikogyo.co.jp

Journal of the Magnetics Society of Japan
Vol. 42, No. 1

Electronic Journal URL: https://www.jstage.jst.go.jp/browse/msjmag

CONTENTS

J. Magn. Soc. Jpn., **42**, 1-4 (2018)

<Paper>

Optimum conditions for synthesizing Fe substituted hibonite

H. Nagumo, K. Kakizaki, and K. Kamishima
Graduate School of Science and Engineering, Saitama University, *255 Shimo-Okubo, Saitama 338–0825, Japan*

We investigated the synthesis conditions and magnetic properties of Fe substituted hibonite with initial compositions of $CaAl_xFe_{y-x}O_{19-\delta}$ ($1 \le x \le 3$, $5 \le y \le 9$) and $CaAl_xFe_{8-x}O_{19-\delta}$ ($0.5 \le x \le 1.6$) sintered at 1200–1300ºC. The optimum conditions for synthesizing the best magnetic hibonite were found to be the initial composition of Ca:Al:Fe = 1:0.6:7.4 and the sintering temperature of 1250ºC. The best magnetic hibonite was magnetized at 75.0 A·m²/kg at T = 5 K and $\mu_0 H$ = 7 T. This magnetic moment can be interpreted with a model of the collinear magnetic structure. The Curie temperature of the best magnetic hibonite was 330ºC, which was the highest among those of iron-substituted hibonite samples.

Keywords: M-type, hexaferrite

1. Introduction

Ca-based M-type ferrite has been attracting a lot of interest because the other alkaline-earth-based M-type ferrites (Ba, Sr)$Fe_{12}O_{19}$ have been used as a permanent magnet for a long time.[1-3] In spite that pure M-type $CaFe_{12}O_{19}$ phase does not exist in the CaO-Fe_2O_3 diagram,[4-6] the M-type phase becomes stable with the addition of a rare-earth element of lanthanum to $CaFe_{12}O_{19}$.[7,8] The optimum synthesis condition of the (Ca,La)-based M-type ferrite with the highest magnetization was recently clarified.[9]

Resources of rare-earth elements are, however, limited in comparison with those of the other elements of calcium, iron, and oxygen. Therefore, it is desirable to avoid the use of rare-earth elements in the material.

On the other hand, the crystal structure of M-type ferrite is similar to that of hibonite ($CaAl_{12}O_{19}$). Therefore, instead of lanthanum, aluminum can stabilize the M-type structure even with iron elements. This approach is consistent with "element strategy" because aluminum, calcium, iron, and oxygen are abundant elements in Earth's crust.[10]

We previously reported the study of synthesis and magnetic properties of Fe substituted hibonite.[11] In this report, we changed initial composition from $CaAl_{12-x}Fe_xO_{19}$ to $CaAl_{10-x}Fe_xO_{19-\delta}$ in order to prevent the excess of α–Fe_2O_3 and to improve the magnetic properties. But it was insufficient to optimize synthesis conditions because α-Fe_2O_3 still remained in the magnetic samples of $CaAl_{10-x}Fe_xO_{19-\delta}$.

In this study, we have investigated the optimum synthesis conditions and magnetic properties of Fe substituted hibonite in order to produce a rare-earth-free Ca-based ferromagnet.

2. Experimental procedure

Samples were prepared by a conventional ceramic method. We used $CaCO_3$, Al_2O_3, and α-Fe_2O_3 as starting materials. First, Al_2O_3 powder was heated at 500ºC for an hour in order to remove water molecules on the material. The starting materials were mixed in the desired proportions of $CaAl_xFe_{y-x}O_{19-\delta}$ ($1 \le x \le 3$, $5 \le y \le 10$) and $CaAl_{8-x}Fe_xO_{19-\delta}$ ($6.4 \le x \le 7.5$) in a ball-milling pot for 24 h. The mixed powder was pressed into a disk shape. The disk was pre-sintered in air at 900ºC for 5 h. The sintered sample was pounded in a mortar and then ground into fine powder using a planetary ball mill for 10 minutes at 1100 rpm (Fritsch, P-7 Premium line). The powder was pressed into a disk shape again. The disks were heated at 1100–1400ºC for 5 h. X-ray diffraction (XRD) analysis with Cu-Kα radiation was performed to characterize the crystalline samples. The magnetic properties were measured by using a vibrating sample magnetometer (Tamakawa TM-VSM2130HGC) and superconducting quantum interference device (SQUID) magnetometers (Quantum Design MPMS-XL). The chemical composition was examined through energy dispersive X-ray analysis (EDX).

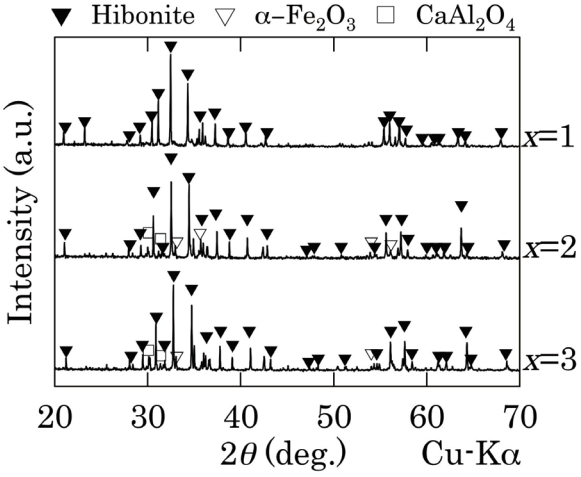

Fig. 1 X-ray diffraction patterns of initial composition samples of $CaAl_xFe_{y-x}O_{19-\delta}$ ($1 \le x \le 3$, y = 8) sintered at T_S = 1300ºC.

3. Results and discussion

Figure 1 shows the X-ray diffraction patterns of the Ca:Al:Fe = 1:x:y–x ($1 \le x \le 3$, $y = 8$) composition samples sintered at T_S = 1300ºC. The sample with the initial composition at x = 1 and y = 8 showed the single hibonite phase. The diffraction pattern of hibonite is almost identical to that of Sr-based M-type ferrite. The other samples of x = 2 and 3 contained minority phases of α-Fe_2O_3 and $CaAl_2O_4$ although the main phase was that of hibonite. This situation is same for other starting composition samples with Ca:Al:Fe = 1:x:y–x ($1 \le x \le 3$, $5 \le y \le 9$). But the single hibonite phase was observed only for the sample at x = 1 and y = 8.

Figure 2 shows the room-temperature saturation magnetization (M_S) of initial composition samples of $CaAl_xFe_{y-x}O_{19-\delta}$ ($1 \le x \le 3$, $5 \le y \le 12$) sintered at T_S = 1300ºC, where M_S was estimated from the magnetization measurements at $-2\ \mathrm{T} \le \mu_0 H \le 2\ \mathrm{T}$. The sample at x = 1 and y = 8 had the highest M_S among these samples. This is consistent with the fact that the sample at x = 1 and y = 8 contained no minority phases of α-Fe_2O_3 and $CaAl_2O_4$.

These experimental results of $CaAl_xFe_{y-x}O_{19-\delta}$ strongly suggest that the suitable (Al+Fe)/Ca ratio is 8 for the formation of the iron-substituted magnetic hibonite. This led us to the next experiments to determine the optimum Al:Fe ratio so as to synthesize the best magnetic hibonite with the highest magnetization and the highest Curie temperature.

Figure 3 shows the X-ray diffraction patterns of initial composition samples of $CaAl_xFe_{8-x}O_{19-\delta}$ ($0.5 \le x \le 1.6$) sintered at T_S = 1250ºC. The maximum iron substitution amount corresponds to x_{max} = 0.6 where the secondary phase of hematite was not left. Here, the sintering temperature T_S was decreased to 1250ºC from 1300ºC because the samples sintered at T_S = 1300ºC showed the secondary hematite phase at x < 1.0. High T_S can remove iron and calcium elements from the hibonite structure with high concentration of Fe^{3+}, possibly due to a low melting point of $CaFe_2O_4$. On the other hand, the single hibonite phase was not observed for the samples at $T_S \le 1225$ºC, suggesting the lowest limit of T_S for the formation of the single phase of hibonite.

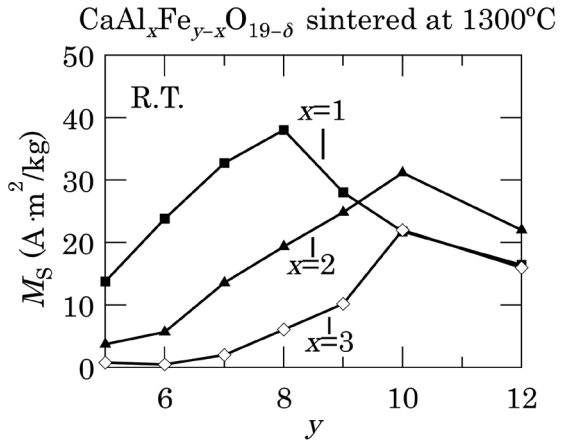

Fig. 2 Room-temperature saturation magnetization of initial composition samples of $CaAl_xFe_{y-x}O_{19-\delta}$ ($1 \le x \le 3$, $0 \le y \le 12$) sintered at T_S = 1300ºC.

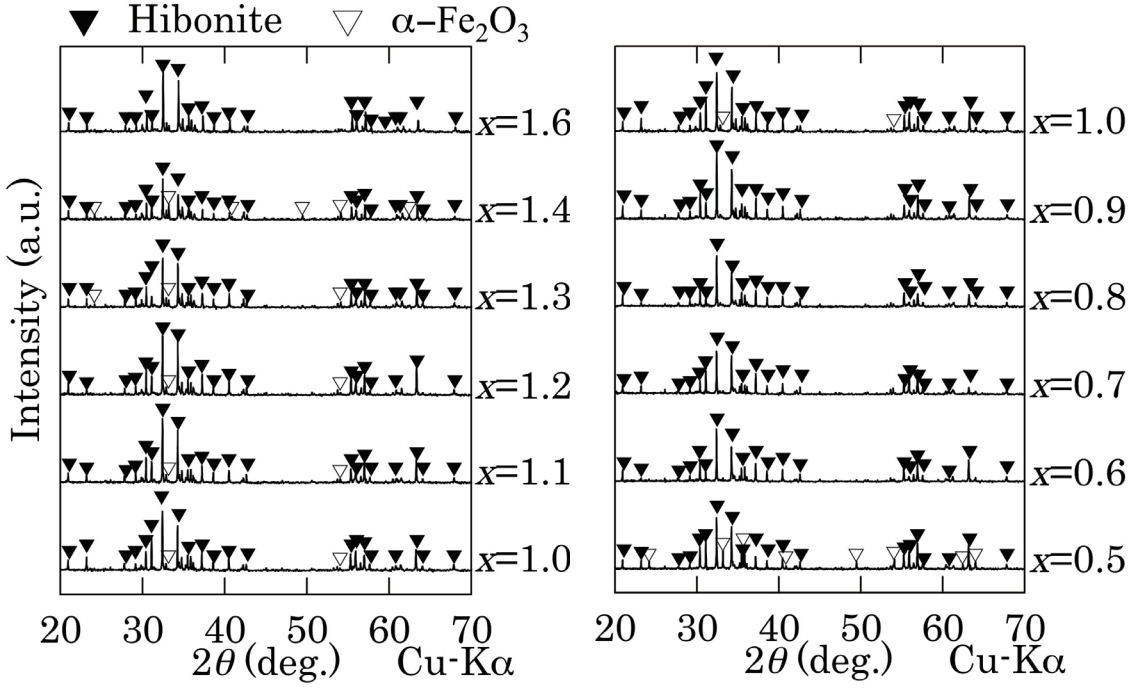

Fig. 3 X-ray diffraction patterns of initial composition samples of $CaAl_xFe_{8-x}O_{19-\delta}$ ($0.5 \le x \le 1.6$) sintered at T_S = 1250ºC.

Figure 4 shows the lattice constants of the hibonite phase in initial composition samples of $CaAl_xFe_{8-x}O_{19-\delta}$ ($0.5 \leq x \leq 1.6$) sintered at T_S = 1250°C. The lattice constants of a and c were obtained by the use of Cohen's least square method.[12] Both a and c became maximum at x = 0.6, which is in agreement with the above-mentioned x_{max}. The maximum lattice constants at x = 0.6 implied that Fe^{3+} ions maximally replaced Al^{3+} ions in the hibonite structure because the ionic radius of an Fe^{3+} ion $r[Fe^{3+}]$ is larger than that of an Al^{3+} ion $r[Al^{3+}]$.

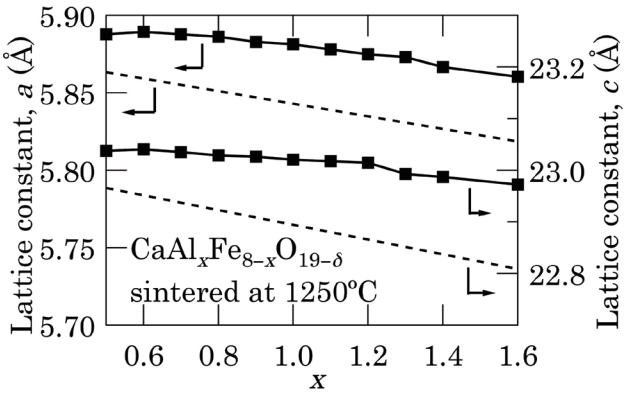

Fig. 4 Lattice constants of initial composition samples of $CaAl_xFe_{8-x}O_{19-\delta}$ ($0.5 \leq x \leq 1.6$) sintered at T_S = 1250°C. Dotted lines are connected between lattice constants of $CaAl_{12}O_{19}$ at x = 8 and those of $SrFe_{12}O_{19}$ (instead of $CaFe_{12}O_{19}$ that does not exist) at x = 0, where a conversion of $x = 8x'/12$ is employed for $CaAl_{12-x'}Fe_{x'}O_{19}$ due to the change of (Al+Fe)/Ca from 12 to 8.

Figure 5 shows the room-temperature saturation magnetization (M_S), the Curie temperature (T_C) and the relative intensity $I^{\alpha-Fe_2O_3}_{(102)}/I^{hibonite}_{(203)}$ of initial composition samples of $CaAl_xFe_{8-x}O_{19-\delta}$ ($0.5 \leq x \leq 1.6$). With decreasing x from 1.6, T_C was linearly increased up to 330°C at x = 0.6 and then slightly decreased at x = 0.5. This x dependence of T_C is comparable to the variation of the lattice constants as shown in Fig. 4. The highest T_C strongly suggests that the sample with x = 0.6 sintered at 1250°C contains the maximum amount of iron cations in the hibonite structure. Also, M_S was basically increased with decreasing x from 1.6 to 0.6 except that M_S deviated from this linear tendency at x = 1.4 and 1.3 because of the formation of a minority phase of α–Fe_2O_3. The sample with x = 0.6 had the maximum M_S of 44 A·m²/kg and the highest T_C of 330°C.

The EDX analysis of the sample with x = 0.6 provides the result of Ca:Al:Fe = 1.00±0.04 : 0.62±0.04 : 7.81±0.23 (average value ± one sigma estimation). The composition of Fe is slightly larger than the initial amount, which may be caused by low-melting-point calcium-iron oxides such as $CaFe_2O_4$ that can be eluted off from the hibonite grain. The chemical formula of this sample can be expressed as $CaAl_{0.6}Fe_{7.8}O_{13.6}$ where the composition ratio of oxygen is estimated from the charge balance with the concentration of Ca^{2+}, Al^{3+}, and Fe^{3+} cations. The form of this chemical formula is much different from the reference materials of hibonite ($CaAl_{12}O_{19}$) and M-type ferrite ($SrFe_{12}O_{19}$).

On the other hand, the x dependences of the lattice constants are similar to the dotted lines connected between lattice constants of $CaAl_{12}O_{19}$ and those of $SrFe_{12}O_{19}$ as shown in Fig. 4. This fact suggests that the framework of the hibonite structure is maintained even in the change of (Al+Fe)/Ca ratio. The crystal structure consists of a close-packed framework of large ions (Ca^{2+} and O^{2-}) with intervening small ions (Al^{3+} and Fe^{3+}). Therefore, we can assume that the total number of large ions (Ca^{2+} and O^{2-}) in the hibonite structure is kept at 20 (= 1+19). Based on this assumption, the chemical formula of the sample with x = 0.6 is estimated to be $Ca_{1.4}Al_{0.8}Fe_{10.7}O_{18.6}$. The total number of Al^{3+} and Fe^{3+} cations becomes 11.5 that is smaller than 12.

This picture can be applied to the case of Al-substituted (Ca,La)-based M-type ferrite. Shigemura *et al.* recently reported that the Curie temperature of $Ca_{0.88}La_{0.12}Fe_{8.80}Al_{1.01}O_{15.8}$ was about 350°C.[13] This chemical formula can be converted to $Ca_{1.05}La_{0.14}Fe_{10.5}Al_{1.20}O_{18.8}$ on the assumption that the total number of large ions (Ca^{2+}, La^{3+}, and O^{2-}) is kept at 20. The estimated amounts of Fe^{3+} in chemical formulas

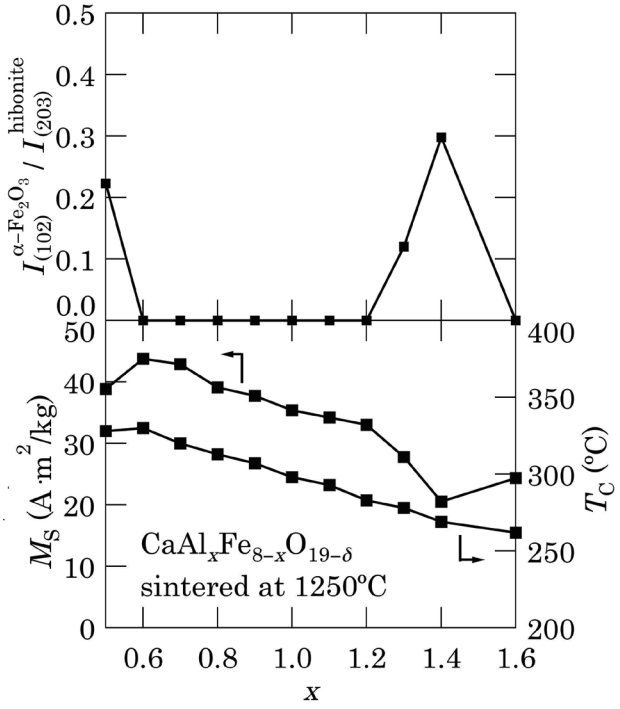

Fig. 5 Room-temperature saturation magnetization (M_S) and Curie temperature (T_C) of initial composition samples of $CaAl_xFe_{8-x}O_{19-\delta}$ ($0.5 \leq x \leq 1.6$) sintered at T_S = 1250°C. Intensity ratio of α-Fe_2O_3 (102) plane to hibonite (203) plane is also shown.

are similar between $Ca_{1.4}Al_{0.8}Fe_{10.7}O_{18.6}$ and $Ca_{1.05}La_{0.14}Fe_{10.5}Al_{1.20}O_{18.8}$, which may cause the similarity in the Curie temperature.

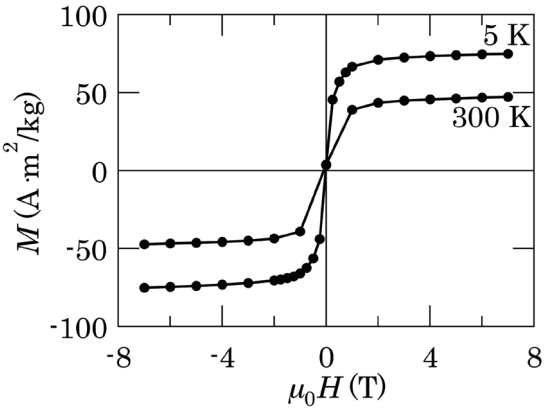

Fig. 6 Magnetization curves at T = 5 K and 300 K for sample at x = 0.6 sintered at T_S = 1250°C.

Figure 6 shows the magnetization curves at T = 5 K and 300 K for the sample with x = 0.6 sintered at T_S = 1250°C. Gradual increase of magnetization was observed above $\mu_0 H$ > 2 T. At the maximum external magnetic field of $\mu_0 H$ = 7 T, the magnetizations at T = 5 K and 300 K are 75.0 A·m^2/kg and 47.3 A·m^2/kg, respectively. The magnetization at T = 5 K corresponds to the magnetic moment per formula unit of 13.1 μ_B/f.u.

We would like to discuss the magnetic structure of the best magnetic hibonite in our study. The magnetic structure of this iron-substituted hibonite can be similar to that of the M-type ferrite because the crystal structure of hibonite is similar to that of the M-type ferrite. The M-type ferrite has a collinear magnetic structure where eight of the Fe^{3+} cations are antiparallel to the other four Fe^{3+} cations. The total magnetic moment of the M-type ferrite is equivalent to four Fe^{3+} cations (20 μ_B).

Here, the chemical formula of the best magnetic hibonite is estimated to be $Ca_{1.4}Al_{0.8}Fe_{10.7}O_{18.6}$. Albanese demonstrated that Al^{3+} cations in $BaAl_xFe_{12-x}O_{19}$ tend to occupy the up-spin 12k site at $x \leq 1$.[14] Also, the estimated chemical formula with the excess of Ca^{2+} cations suggests that Ca^{2+} replaces O^{2-} (possibly in the R-block), which can produce vacancy at a small cation site due to the local electroneutrality (the Pauling principle). Therefore, we can assume that the magnetic hibonite has the collinear magnetic structure where the up-spin-sites contain 0.8 Al^{3+} and 0.5 vacancy. Then, 6.7 Fe^{3+} cations are antiparallel to the other four Fe^{3+} cations. The total magnetic moment of the magnetic hibonite becomes equivalent to 2.7 Fe^{3+} cations (13.5 μ_B). This value is close to the experimental result of 13.1 μ_B/f.u. at T = 5 K and $\mu_0 H$ = 7 T.

The slight difference between the experimental result and the estimated value can be caused by the deviation from the collinear magnetic structure. In fact, Batlle *et al.* pointed out that the substitution of Co^{2+}-Ti^{4+} for Fe^{3+} in $BaFe_{12}O_{19}$ can progressively break the collinearity of the magnetic structure of $BaFe_{12-2x}Co_xTi_xO_{19}$ at x > 0.7 although the overall behavior remains ferrimagnetic.[15] In our case, the collinearity of our sample can be also weakened because the estimated amount of the Fe^{3+} cations in our sample is close to this threshold of 10.6 (= 12–2×0.7) and our sample does not contain magnetic Co^{2+} cations. The high-field susceptibility of our sample is relatively high as shown in Fig. 6, suggesting the weakened collinearity.

Therefore, our result is consistent with the previous studies of M-type ferrite.

4. Conclusion

We have successfully synthesized Fe^{3+} substituted hibonite–phase samples by a conventional ceramic method. The optimum synthesis conditions of the best magnetic hibonite are found to be the initial composition of Ca:Al:Fe = 1:0.6:7.4 and the sintering temperature of 1250°C. The magnetization of the best magnetic hibonite was 75.0 A·m^2/kg at T = 5 K and $\mu_0 H$ = 7 T. This magnetic moment can be basically interpreted with the model of the collinear magnetic structure. The Curie temperature of the best magnetic hibonite was 330°C, which is the highest among those of iron-substituted hibonite samples.

References

1) J. Smit and H. P. J. Wijn: Ferrites, pp. 182–184, pp. 193–194 (Philips Technical Library, Netherlands 1959).
2) S. Chikazumi: Physics of Ferromagnetism, p. 210 (Oxford University Press, Oxford, 2009).
3) Ü. Özgür, Y. Alivov, and H. Morkoc: *J. Mater. Sci-Mater. El.*, **20**, 789 (2009).
4) B. S. Boyanov: *J. Min. Met.*, **41 B**, 67 (2005).
5) M. Hillert, M. Selleby, and B. Sundman: *Metall. Trans. A*, **21A**, 2759 (1990).
6) B. Philips and A. Muan: *J. Am. Ceram. Soc.*, **41**, 445 (1958).
7) N. Ichinose and K. Kurihara: *J. Phys. Soc. Jpn.*, **18**, 1700 (1963).
8) H. Yamamoto, T. Kawaguchi, and M. Nagakura: *IEEE Trans. Magn.*, **15**, 1141 (1979).
9) M. Shigemura, K. Watanabe, K. Kakizaki, and K. Kamishima: *J. Magn. Soc. Jpn.*, **41**, 10 (2017).
10) F. W. Clarke and H. S. Washington: The Composition of the Earth's Crust, pp. 20–21 (United States Geological Survey, Washington, 1924).
11) H. Nagumo, K. Watanabe, K. Kakizaki and K. Kamishima: *J. Magn. Soc. Jpn.*, **41**, 20 (2017).
12) B. D. Cullity: Elements of X-ray Diffraction, 342 (Addison-Wesley, 1967).
13) M. Shigemura, K. Kakizaki, and K. Kamishima: J. Magn. Soc. Jpn., **41**, 94 (2017).
14) G. Albanese: *J. Magn. Magn. Mater.*, **147**, 421 (1995).
15) X. Batlle, X. Obradors, J. Rodríguez-Carvajal, M. Pernet, M. V. Cabañas, M. Vallet: *J. Appl. Phys.*, **70**, 1614 (1991).

Received Jun. 18, 2017; Revised Aug. 8, 2017; Accepted Oct. 30, 2017

J. Magn. Soc. Jpn., **42**, 5-10 (2018)

<Paper>

AC Magnetic Field Imaging of Perpendicular Magnetic Write Head without Image Distortion on Alternating Magnetic Force Microscopy using a Cone-Shape FePt-coated Tip

S. Yoshimura[1], F. Zheng[2,3], S. Yasui[1], G. Egawa[1], and H. Saito[1]

[1]Research Center for Engineering Science, Graduate School of Engineering Science, Akita University, *Tegata Gakuen-machi 1-1, Akita 010-8502, Japan*

[2]Venture Business Laboratory, Akita University, *Tegata Gakuen-machi 1-1, Akita 010-8502, Japan*

[3]School of Physics and Electronic-Electrical Engineering, Ningxia University, *Yinchuan 750021, China*

The AC magnetic field of a perpendicular magnetic write head having three surrounding shields was successfully imaged without image distortion on our alternating magnetic force microscope (A-MFM) using a newly developed cone-shape Si tip coated with an $L1_0$-FePt film. In contrast, a conventional quadrangular pyramidal Si tip coated with the $L1_0$-FePt film showed a distortion of the AC magnetic field image for the same magnetic write head. The image distortion depended on the spatial configuration between the tip and the write head. It is concluded that a round magnetic symmetry of the cone-shape FePt-coated tip is most effective for taking a clear AC magnetic field image of the perpendicular magnetic write head having three surrounding shields without distortion.

Key words: perpendicular magnetic write head, alternating magnetic force microscopy, image distortion, cone-shape FePt-coated tip

1. Introduction

In perpendicular magnetic recording, the demand for high magnetic recording density requires the super performance of magnetic recording media and magnetic write/read head. To achieve high recording density, the write head design has to be optimized to achieve the large field magnitude and a high field gradient in both the down-track and cross-track directions as required. So far, most characterizations of the magnetic field of write head have been done by theoretical modeling[1)-4)]. However, the simulation of the exact working conditions of a write head in a drive has encountered difficulty when using theoretical modeling. At the same time, the characterization of write head has been done by experimental spin-stand measurements. The results obtained from this spin-stand measurement not only include the effect of the real magnetic field distribution of the write head, but also the magnetic property and microstructure of the recording media.

Magnetic force Microscope (MFM) is a powerful tool to understand the microscopic magnetic domain/bit structures of high density magnetic recording media and nanoscale magnetism[5)]. The maximum resolution of an MFM is approximately 10 nm[6)]. For this reason, MFM applications for the development of magnetic materials and magnetic devices have received more and more attention over the past ten years.

To detect and image an AC magnetic field, the conventional MFM has to employ a frequency which is close to the mechanical resonant frequency of the MFM cantilever[7),8)]. Because the cantilever acts as a mechanical filter near its resonant frequency, the signals at the frequencies that are not close to the cantilever's resonant frequency will not be picked up.

In our previous work, we have developed a new MFM to image AC magnetic field with a wide frequency range that is referred to as alternating magnetic force microscopy (A-MFM)[9)]. The A-MFM uses a frequency modulation (FM) of the cantilever oscillation by applying an AC magnetic field over it. The A-MFM can measure the vertical component of an AC magnetic field when the magnetization direction of MFM tip is perpendicular to the sample surface. Previously, we achieved high-resolution AC magnetic field images for a perpendicular magnetic write head having a one-side trailing shield by such A-MFM with a conventional quadrangular pyramidal FePt-coated tip[10),11)]. The $L1_0$-FePt film having a coercivity of more than 10 kOe has been used for the MFM tip in this case, because the magnetic field from the write head is overly strong to be able to change magnetization of an MFM tip. The development of MFM tips coated with hard magnetic materials such as Fe-Pt[12)-16)], Fe-Pd[16),17)], Co-Pt[18)-22)], and Sm-Co[23)] were reported by several groups. However, the shape effect of the MFM tip with hard magnetic coatings has barely taken into account.

In the present study, we developed a new FePt-coated tip with a special shape for the characterization of a perpendicular magnetic recording head having three surrounding shields. The head design having three surrounding shields can generate more focused magnetic field for high recording density. The conventional quadrangular pyramidal shape tip with FePt coating usually causes image distortion for this type of head. The newly-developed tip was

supposed to fix the issue with the image distortion of the AC magnetic field. The image distortion is defined as the disaccord between the position, shape, and spatial symmetry of main pole in topographic image and those of strong signal in amplitude image of A-MFM. We analyzed the cause for the image distortion of the AC magnetic field when using the quadrangular pyramidal-shape tip and found the way to make the AC magnetic field successfully imaged without distortion by using the developed FePt-coated tip. In this paper, we will also show a necessity to increase the coercivity of hard magnetic coating to characterize future perpendicular magnetic write head.

2. Experimental Procedure

The A-MFM was built from a conventional scanning probe microscope (JSPM-5400 (JEOL Ltd.) and/or SPI3800N・SPA300HV (SII-NT Ltd.)). All of the measurements were done in air atmosphere. The cantilever was oscillated by using a piezoelectric element. The value of the resonant frequency of the cantilever with the MFM tip was approximately 330 kHz. The oscillation frequency (f_c) of the piezoelectric element was set at 325 kHz which is close to the resonant frequency of the tip, and the value of Q was around 500.

A perpendicular magnetic write head having a one-side trailing shield and a perpendicular magnetic write head having three surrounding shields were sampled for this work. The write head was driven by a sinusoidal AC current with a zero-to-peak amplitude of 20 or 40 mA at the frequency (f_m) of 100 Hz.

The AC magnetic field frequency modulated the cantilever resonant frequency. The cantilever deflections were sensed by using laser beam deflection. The AC magnetic field measurement was achieved by the lift mode after topographic measurement. The lift height was 10 nm. The amplitude and phase information of the alternating force between the sample and the tip was extracted by using a lock-in amplifier where the input signal was the frequency demodulated signal of cantilever oscillation from a phase-locked loop (PLL) circuit and reference signal was the frequency signal of f_m from signal generator[8),9)].

Both conventional high-coercivity MFM tip (SI-MF40-Hc, Nitto Optical Co. Ltd.) with a quadrangular pyramidal shape (DF-40, SII Co. Ltd.) and a 30 nm-thick $L1_0$-FePt coating, and a new made-in-house MFM tip in cone-shape (SS-ISC, Team Nanotec Co. Ltd.) coated with the same thickness $L1_0$-FePt film were used in this work. The MFM tips were magnetized to saturation along the tips axis before use to make sure the magnetization direction of the tips were vertical to the write head surface.

3. Results and Discussions

First, the quadrangular pyramidal FePt-coated tip was used to take the amplitude and phase images of the AC magnetic field of the two types of write heads. Fig.1 shows SEM images of the quadrangular pyramidal Si tip. Fig.1 (a) is an image of entire tip, Fig.1 (b) a magnified image of the vertex region of the tip, and Fig.1 (c) a top view of the vertex region of the tip.

The results for the head having a one-sided trailing shield and the head having three surrounding shields are shown in the topographic image in Fig.2 (a) and (d), respectively. Fig.2 (b) and (c) are the amplitude and the phase images of the AC magnetic field for the head having a one-sided trailing shield, respectively. Fig.2 (e) and (f) are the amplitude and phase images for the head having three surrounding shields, respectively. In all measurements the AC current was fixed at 20 mA.

For the head having a one-side trailing shield, the amplitude and the phase images of the AC magnetic field are clearly observed without distortion. In Fig.2 (b), the strong amplitude of the AC magnetic field (bright area) appears at the main pole position. In addition, a relatively large field intensity is obtained at the trailing shield position near the gap, and a very low intensity of near-zero is obtained at the gap position. In Fig.2 (c), the polarity of the field can be clearly observed as a binary image. The phase difference between the dark area and bright area is approximately 180°. If the dark area corresponds to the in-phase magnetic field with respect to the head current, the bright area corresponds to the field in the opposite direction. As shown in this figure, the polarity of the perpendicular component of the AC magnetic field at the main pole region and the trailing shield region of the head can be clearly distinguished. The AC magnetic field images were clearly observed without obvious distortion for the write head having a one-sided trailing shield.

In contrast, the image of the strong amplitude of the AC magnetic field (bright area) around the main pole position becomes asymmetric on certain direction

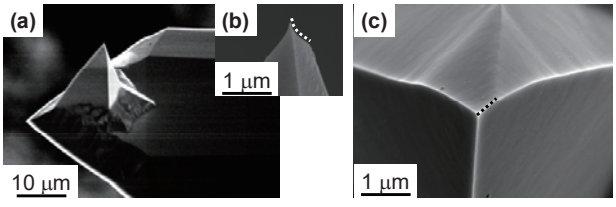

Fig. 1 SEM images of quadrangular pyramidal Si tip: (a) entire tip, (b) magnified image of vertex region of the tip, and (c) top view of vertex region of the tip. The dotted line in (b) and (c) indicates the ridges from the 1st vertex to the 2nd vertex of the tip.

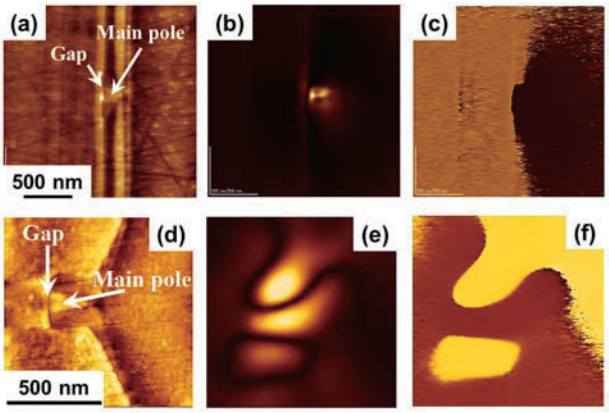

Fig. 2 (a) and (d) are topographic images, (b) and (e) are amplitude images of the AC magnetic field, and (c) and (f) are phase images of the AC magnetic field. (a), (b), and (c) are images for the write head having a one-sided trailing shield, and (d), (e), and (f) are images for the write head having surrounding shields on three sides.

as shown in Fig.2 (e). In addition, a near-zero intensity is not observed at the gap position. In Fig.2 (f), the polarity of the field observed around the main pole position is also asymmetric in certain direction. A polarity change of the field could not be observed at the gap position.

The observations above hints at a distortion of the amplitude and the phase images for a head having three surrounding shields. To investigate the cause for the distortion of the AC magnetic field images, the shape effect of the quadrangular pyramidal FePt tip was taken into account. This tip has two vertices, and the dot line in Fig.1 (b) and (c) indicates the ridge line formed by the 1st vertex and the 2nd vertex of the tip. This ridge line is one possible factor contributing to the image distortion, the ambiguity at the gap position, and the asymmetry of the field images.

To clarify the influence of the ridge line of the tip on the AC magnetic field imaging, the spatial configuration between the quadrangular pyramidal FePt-coated tip and the write head having three surrounding shields was adjusted and imaged the AC magnetic field images. Fig.3 (a), (d), and (g) show schematics of the quadrangular pyramidal FePt-coated tip and the spatial configurations against the write head. The dotted line and bold line in (a), (d), and (g) indicate the outline and the ridge line formed by the 1st vertex and the 2nd vertex of the tip, respectively. Fig.3 (b), (e), and (h) show the corresponding amplitude images of the AC magnetic field, and Fig.3 (c), (f), and (i) show the corresponding phase images of the AC magnetic field for the write head. In the case of Fig.3 (g), the direction of the ridge line (bold line) is parallel to the direction of the cross-track of the write head. The (h) amplitude and (i) phase images of the AC magnetic field extend toward the direction of the

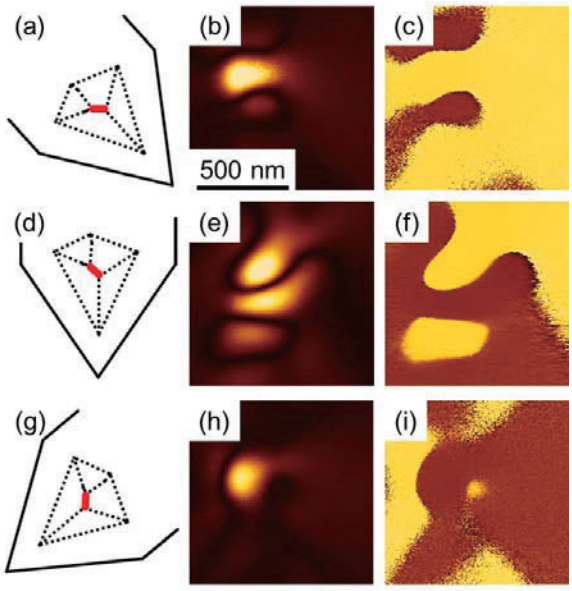

Fig. 3 (a), (d), and (g) are the schematics of the quadrangular pyramidal FePt tip and its spatial configuration against the writing head, (b), (e), and (h) are the amplitude images, and (c), (f), and (i) are the phase images of the AC magnetic field for the writing head having three surrounding shields.

cross-track of the write head. These results suggest that the image distortion of the AC magnetic field depends on the spatial configuration between the tip and the write head. Here, the (e) amplitude and (f) phase images of the AC magnetic field were already discussed in Fig.2 (e) and (f).

Self-magnetic charge of the FePt film happens at the edge line of film surface. As a result, the magnetic pole line is created at each ridgeline of the tip and the center part of the tip end. The center part of the tip end mainly contributes to the signal for the AC magnetic field image in direction perpendicular to the ridge line of the tip, while the ridge lines of the tip mainly generate the signal for the AC magnetic field image in direction parallel to the ridge lines of the tip.

In order to reduce the influence of ridge pole line on imaging AC magnetic field, a new tip having a cone-shape was developed. Fig.4 shows SEM images of the cone-shape Si tip. Fig.4 (a) is the image of the entire tip, (b) is the magnified image of the vertex of the tip, and (c) is the top view of the vertex of the tip. This tip has only one vertex with a round symmetry. Within this cone-shape tip, the magnetic pole of FePt film forms only at the end of the tip. To see the influence of the improved round symmetry of the tip magnetics on the image distortion, the cone-shape FePt-coated tip was used for the characterization of the write head having three surrounding shields. Fig.5 show (a) a schematic of the cone-shape FePt-coated tip and its spatial configuration against the write head, (b) the topographic image, and (c) the amplitude and (d)

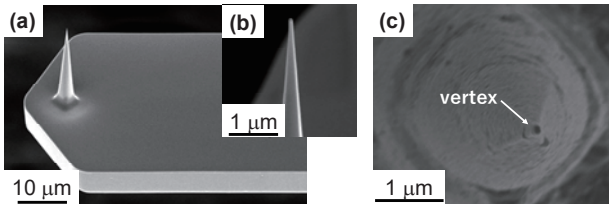

Fig. 4 SEM images of the cone-shape Si tip: (a) image of entire tip, (b) magnified image of vertex region of the tip, and (c) top view of vertex region of the tip.

phase images of the AC magnetic field of the write head having three surrounding shields. The dot line and bold point in (a) indicate the outline and the end point of the tip, respectively. The amplitude and the phase images of the AC magnetic field are clearly observed without image distortion. In Fig.5 (c), a strong intensity, relatively large intensity, and very low intensity of nearly zero can be seen at the main pole position, the trailing shield position near the gap, and the gap position, respectively. In Fig.5 (d), the polarity of the field can be observed clearly. The phase difference between the main pole and the three surrounding shields is approximately 180°. It is clear that the amplitude and phase images of the AC magnetic field are not distorted for the write head having three surrounding shields.

As described earlier, there was no image distortion observed for the head having one-side trailing shield by using the quadrangular pyramidal FePt-coated tip. The magnetic field of the head having one-side trailing shield is not strong enough compared with that of the head having three surrounding shields, and mainly focuses at the 1st vertex region of the tip. Moreover, the shape of the quadrangular pyramidal tip around the 1st vertex has a near-cone shape from the detail

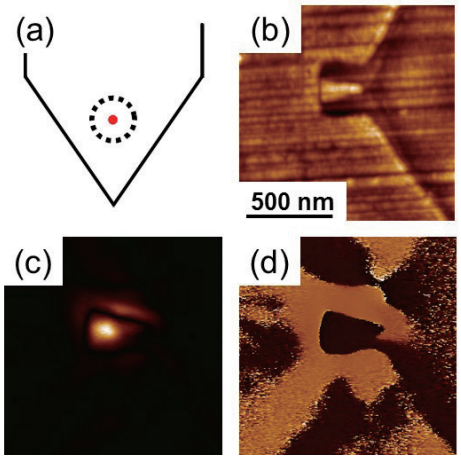

Fig. 5 (a) is a top view of the cone-shaped FePt tip, (b) is a topographic image, (c) is an amplitude image, and (d) is a phase image of the AC magnetic field for the write head with three surrounding shields.

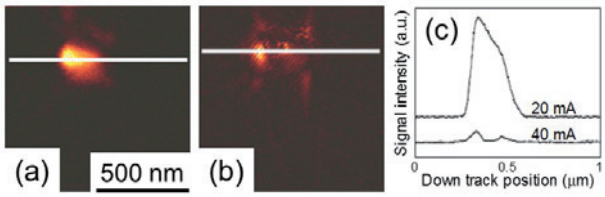

Fig. 6 (a) and (b) are the amplitude images of AC magnetic field for the write head having three surrounding shields at the head driving current of 20 mA and 40 mA, respectively. (c) is the down track line profile of amplitude signal of the white line shown in (a) and (b).

SEM observation. Therefore, the MFM measurement of the write head having one-side trailing shield by using the quadrangular pyramidal FePt-coated tip is almost same situations as that of the write head having three surrounding shields by using the cone shape FePt-coated tip. On the other hand, the magnetic field of the head having three surrounding shields focuses not only at the 1st vertex region but also the ridgeline of the quadrangular pyramidal tip. This is why the AC magnetic field image of the write head having three surrounding shields shows no distortion when using the cone-shape FePt-coated tip. This means that the MFM tip with round symmetry for the magnetic pole charge is very important to reduce image distortion when characterizing strong, widely-spread magnetic field generated from a write head. These results generally indicate that the MFM tip with asymmetry for the magnetic charge is effective to get a MFM image without distortion only for the case of samples which generate the not so strong and widely-spread magnetic field.

A sinusoidal AC current of 20 mA with a zero-to-peak amplitude was used for the above A-MFM characterization of the magnetic write head. This is smaller than that of the actual motion of magnetic write head working in hard disk drive.

Fig.6 (a) and (b) show the amplitude images of AC magnetic field taken by the cone-shape FePt-coated tip with a film thickness of 40 nm for the write head having three surrounding shields. In this run, the head driving current of 20 mA and 40 mA were applied respectively. Fig.6 (c) is the down track line profile of amplitude signal of the white line shown in Fig.6 (a)

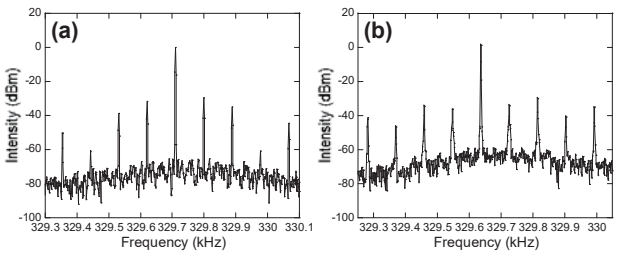

Fig. 7 Spectra of the cantilever oscillation with the head current of (a) 20 mA and (b) 40 mA.

and (b). The amplitude image (a) and its line profile for the head current of 20 mA were clear with a high amplitude signal at the main pole position. In comparison, the amplitude image (b) and its line profile for the head current of 40 mA were unclear and very low amplitude signal at the main pole position. Especially, there is an amplitude signal of near-zero with the head current of 40 mA at the position which has the highest amplitude signal with head current of 20 mA. These indicate that the magnetization state of the magnetic tip is different between the head currents of 20 mA and 40 mA.

To understand the difference of signal intensity with different head running currents, the measurement of frequency spectra of tip oscillation for each head current was carried out by using spectrum analyzer. Fig.7 (a) and (b) show the spectra of the tip oscillation with the head running current of 20 mA and 40 mA, respectively. The oscillation frequency (f_c) of the tip was 329.71 kHz (on the head current of 20 mA) and 329.64 kHz (on the head current of 40 mA), and the frequency (f_m) of the AC magnetic field 100 Hz. As seen in the figures, the sideband spectra with the frequency of $f_c \pm n f_m$ (n: an integer), which is modulated by AC magnetic field from head, are observed near the baseband spectra of the cantilever oscillation with the frequency of fc. The frequency of $f_c \pm f_m$ is dominating when coercivity of the magnetic component of tip is higher than the AC magnetic field. And the frequency of $f_c \pm 2f_m$ is dominating when coercivity of the magnetic component of the tip is smaller than the AC magnetic field. This is because, the spectrum intensity at $f_c \pm f_m$ is proportional to the gradient of magnetic field component which is perpendicular to the sample surface[9], and this indicates that direction of tip magnetization does not change when the $f_c \pm f_m$ is dominant. In Fig.7 (a), the modulated frequency with highest peak of the spectra was $f_c \pm f_m$. This indicates that hard magnetic behavior of the magnetic tip is dominant in the case of head current of 20 mA. By comparison, the modulated frequency with highest peak of the spectra was $f_c \pm 2f_m$ as shown in Fig.7 (b). This indicates that soft magnetic behavior of the magnetic tip is dominant in the case of head current of 40. The reason for the low amplitude signal at the main pole position in Fig.6 (b) is due to the increment of oscillation intensity at modulated frequency of the $f_c \pm 2f_m$. In addition, the modulated frequencies of $f_c \pm n f_m$ (n>2) were observed in both cases with different intensities. This suggests that the magnetization direction of the FePt tip sways in a non-linear way. It is clear that the coercivity of the FePt coating is lower than the magnetic field generated by the head with the current of 40 mA. The magnetization direction of the FePt tip is swayed by the magnetic field of the head with the current of 20 mA although the coercivity of FePt coating is larger than the head field. Therefore, the increase of tip coercivity is necessary to take accurate MFM images of future magnetic write head. We will describe the effect of increased tip coercivity in a future paper.

4. Conclusion

We analyzed the cause of the MFM image distortion of the AC magnetic field for the magnetic recording heads having 3 surrounding shields by comparing a conventional quadrangular pyramidal FePt-coated tip with our newly developed cone shape FePt-coated tip. The cone shape FePt-coated tip makes it able to image the AC magnetic field of perpendicular magnetic write head having three surrounding shields without image distortion.

In comparison to the quadrangular pyramidal shape structure of the conventional FePt tip, the cone-shape FePt-coated tip and its round magnetic symmetry are very effective in imaging the AC magnetic field of the write head having three surrounding shields without image distortion. In addition, it is necessary to increase the coercivity of hard magnetic coating in order to characterize the very high magnetic field for the future magnetic write head.

Acknowledgements This work was supported by JST/SENTAN.

References

1) Y. Kanai, M. Saiki, and K. Yoshida: *IEEE Trans. Magn.*, **43**, 1665 (2007).
2) Y. Kanai, K Hirasawa, T Tsukamoto, K. Yoshida, S.J. Greaves, and H. Muraoka, *IEEE Trans. Magn.*, **44**, 3609 (2008).
3) M.E. Schabes: *J. Magn. Magn. Mater.*, **320**, 2880 (2008).
4) K. Takano, L. Guan, Y. Zhou, Y. Liu, J. Smyth, and M. Dovek: *J. Appl. Phys.*, **105**, 07B711 (2009).
5) D. Rugar, H. J. Mamin, P. Guethner, S. E. Lambert, J. E. Stern, I. Mc-Fadyen, and T. Yogi: *J. Appl. Phys.*, **68**, 1169 (1990).
6) H. Saito, R. Sunahara, Y. Rheem, and S. Ishio: *IEEE Trans. Magn.*, **41**, 4394 (2005).
7) Z Y. Martin and H. K. Wickramasinghe: *Appl. Phys. Lett.*, **50**, 1455 (1987).
8) M. R. Koblischka, J. D. Wei, and U. Hartmann: *J. Phys.: Conf. Ser.*, **61**, 591 (2007).
9) H. Saito, H. Ikeya, G. Egawa, S. Ishio, and S. Yoshimura: *J. Appl. Phys.*, **105**, 07D524 (2009).
10) W. Lu, Z. Li, K. Hatakeyama, G. Egawa, S. Yoshimura, and H. Saito: *Appl. Phys. Lett.*, **96**, 143104 (2010).
11) W. Lu, K. Hatakeyama, G. Egawa, S. Yoshimura, and H. Saito: *IEEE Trans. Magn.*, **46**, 1479 (2010).
12) Y Rheem, H Saito, and S Ishio: *IEEE Trans. Magn.*, **41**, 3793 (2005).
13) I.C. Chen, L.H. Chen, A. Gapin, S. Jin, L. Yuan, and S.H. Liou: *Nanotechnology*, **19**, 075501 (2008).
14) N. Amos, A. Lavrenov, R. Fernandez, R. Ikkawi, D. Litvinov, and S. Khizroev: *J. Appl. Phys.*, **105**, 07D526 (2009).
15) N. Amos, R. Fernandez, R.M. Ikkawi, M. Shachar, J.M. Hong, B.S. Lee, D. Litvinov, and S. Khizroev: *IEEE Magn. Lett.*, **1**, 6500104 (2010).
16) S. Ishihara, M. Ohtake, and M. Futamoto: *Thin Solid Films*, **546**, 205 (2013).

17) S. Ishihara, M. Ohtake, and M. Futamoto: *EPJ Web Conf.*, **40**, 08003 (2013).
18) S.H Liou and Y.D Yao: *J. Magn. Magn. Mater.*, **190**, 130 (1998).
19) L. Gao, L.P. Yue, T. Yokota, R. Skomski, S.H. Liou, H. Takahoshi, H. Saito, and S. Ishio: *IEEE Trans. Magn.*, **40**, 2194 (2004).
20) S. Ishihara, T. Hagami, K. Soneta, M. Ohtake, and M. Futamoto: *J. Magn. Soci. Jpn.*, **37**, 56 (2013).
21) S. Ishihara, M. Ohtake, and M. Futamoto: *J Magn. Soci. Jpn.*, **37**, 255 (2013).
22) S. Ishihara, M. Ohtake, and M. Futamoto: *EPJ Web Conf.*, **75**, 06007 (2014).
23) V. Neu, T. Sturm, S. Vock, and L. Schultz: *IEEE International Magnetics Conference (INTERMAG Europe 2014)*, EG-6 (2014).

Received Nov. 23, 2016; Accepted Oct. 30, 2017

Editorial Committee Members · Paper Committee Members

Notice for Photocopying

編集委員・論文委員

複写をされる方へ

Journal of the Magnetics Society of Japan

Vol. 42 No. 1 (通巻第 295 号) 2018 年 1 月 1 日発行

Vol. 42 No. 1 Published Jan. 1, 2018
by the Magnetics Society of Japan
Tokyo YWCA building Rm207, 1–8–11 Kanda surugadai, Chiyoda-ku, Tokyo 101–0062
Tel. +81–3–5281–0106 Fax. +81–3–5281–0107

Printed by JP Corporation Co., Ltd.
2–3–36, Minamikase, Saiwai-ku, Kanagawa 212–0055
Advertising agency: Kagaku Gijutsu-sha

発行：（公社）日本磁気学会 101–0062 東京都千代田区神田駿河台 1–8–11 東京YWCA会館 207 号室
製作：ジェイピーコーポレーション 212–0055 神奈川県川崎市幸区南加瀬 2–3–36 Tel.（044）571–5815
広告取扱い：科学技術社 111–0052 東京都台東区柳橋 2–10–8 武田ビル 4F Tel.（03）5809–1132